THE JOURNAL OF BIOLOGICAL CHEMISTRY VOL. 290, NO. 35, pp. 21510–21522, August 28, 2015
Published in the U.S.A.

Prion Protein Prolines 102 and 105 and the Surrounding Lysine Cluster Impede Amyloid Formation*

Received for publication, May 18, 2015, and in revised form, June 29, 2015 Published, JBC Papers in Press, July 14, 2015, DOI 10.1074/jbc.M115.665844

Allison Kraus[‡], Kelsie J. Anson[‡], Lynne D. Raymond[‡], Craig Martens[§], Bradley R. Groveman[‡], David W. Dorward[§], and Byron Caughey[‡1]

From the [‡]Laboratory of Persistent Viral Diseases and [§]Research Technologies Branch, Rocky Mountain Laboratories, NIAID, National Institutes of Health, Hamilton, Montana 59840

Background: We investigated how pathogenic prion protein mutations P102L and P105L lead to misfolding.
Results: Mutations of these proline and adjacent lysine residues accelerated *in vitro* formation of amyloid with properties reminiscent of PrP^{Sc}.
Conclusion: Specific proline and lysine residues might delay spontaneous prion disease by hindering PrP conversion into amyloid.
Significance: These findings suggest mechanisms for genetic prion diseases.

Human prion diseases can have acquired, sporadic, or genetic origins, each of which results in the conversion of prion protein (PrP) to transmissible, pathological forms. The genetic prion disease Gerstmann-Straussler-Scheinker syndrome can arise from point mutations of prolines 102 or 105. However, the structural effects of these two prolines, and mutations thereof, on PrP misfolding are not well understood. Here, we provide evidence that individual mutations of Pro-102 or Pro-105 to noncyclic aliphatic residues such as the Gerstmann-Straussler-Scheinker-linked leucines can promote the *in vitro* formation of PrP amyloid with extended protease-resistant cores reminiscent of infectious prions. This effect was enhanced by additional charge-neutralizing mutations of four nearby lysine residues comprising the so-called central lysine cluster. Substitution of these proline and lysine residues accelerated PrP conversion such that spontaneous amyloid formation was no longer slower than scrapie-seeded amyloid formation. Thus, Pro-102 and Pro-105, as well as the lysines in the central lysine cluster, impede amyloid formation by PrP, implicating these residues as key structural modulators in the conversion of PrP to disease-associated types of amyloid.

The mammalian prion diseases, or transmissible spongiform encephalopathies (TSEs),[2] can have sporadic, genetic, or acquired origins. In all cases, the normal endogenous prion protein, PrP^{C}, is converted to pathological, disease-associated forms (PrP^{D}). The human genetic prion disease Gerstmann-Straussler-Scheinker (GSS) syndrome can be caused by a proline to leucine substitution at PrP residues 102 (P102L) or 105 (P105L) (1, 2). GSS is fatal, untreatable, and characterized pathologically by the accumulation of PrP^{D} aggregates, primarily in the form of amyloid plaques.

A variety of studies using animal and *in vitro* models have confirmed that the P102L or P105L mutations can cause prion disease and affect PrP folding. Transgenic mice overexpressing the mouse equivalent of P102L, Tg(MoPrP-P101L), spontaneously develop disease (3) and serial passage of brains from clinical Tg(MoPrP-P101L) mice into Tg(MoPrP-P101L) mice and wild-type Syrian hamsters in turn caused TSE disease (4). However, the incidence and onset of disease in mice overexpressing MoPrP-P101L are variable (3, 4), and introduction of the P101L mutation into the endogenous murine PrP gene does not result in spontaneous TSE disease (5). A synthetic peptide comprised of amino acids 89–143 containing the mutant P101L residue can convert to a β-rich conformation that causes TSE disease when injected into Tg(MoPrP-P101L) mice (6). The P102L and P105L mutations also decrease the efficiency of lipid-induced 23–230 recombinant PrP (rPrP) conversion to an infectious PK-resistant form *in vitro* (7). The P102L substitution in the PrP(89–143) peptide allows the spontaneous formation of a cross β-fibril (8, 9), and P102L substitution in 23–231 rPrP is known to reduce the α-helical content, suggesting that the P102L substitution has a structural impact (10). However, although the pathogenic potential of the P102L and P105L mutants is evident, Pro-102 and Pro-105 are contained within an intrinsically disordered region of PrP^{C}, and the structural constraints imposed by these proline residues in PrP are not clear. Furthermore, the field has not ascertained the structural role that Pro-102 and Pro-105 play within the central lysine cluster (CLC), a highly conserved region encompassing amino acids 101–110 that modulates cofactor binding (7), PrP conversion (11), and amyloidogenicity (12).

Proline residues impose unique structural constraints on protein secondary structure because the side chain is covalently bound to the preceding nitrogen in the peptide backbone. Thus, proline residues can have distinctive influences on a protein's biological activity. Proline residues can also have a propensity

* This work was supported, in whole or in part, by National Institutes of Health Intramural Research Program of the NIAID. The authors declare that they have no conflicts of interest with the contents of this article.
[1] To whom correspondence should be addressed. Tel.: 406-363-9264; E-mail: bcaughey@nih.gov.
[2] The abbreviations used are: TSE, transmissible spongiform encephalopathy; GSS, Gerstmann-Straussler-Scheinker; POPG, 1-palmitoyl-2-oleoylphosphatidylglycerol; PrP, prion protein; rPrP, recombinant PrP; RT-QuIC, real time quaking-induced conversion; NBH, normal brain homogenate; ScBH, scrapie brain homogenate; CLC, central lysine cluster; Bis-Tris, 2-[bis(2-hydroxyethyl)amino]-2-(hydroxymethyl)propane-1,3-diol; ThT, thioflavin T.

to form a unique extended left-handed helical structure that is often found in loosely folded or flexible protein domains (13). Moreover, proline isomerization (14–16) and the composition of proline *versus* glycine residues are known to influence amyloid assembly (17). Similarly, a peptidyl-prolyl isomerase, Pin1, affects amyloid precursor protein processing (18) and the phosphorylation and aggregation of Tau (19). These findings reinforce the idea that proline residues can modulate conversion of proteins to amyloids. However, the mechanistic underpinnings of how proline residues influence PrP amyloidogenesis have not been elucidated.

Much research has probed the conversion of normal prion protein, PrP^C, to PrP^D, but the structural and mechanistic details remain elusive. The best characterized forms of PrP^D are amyloid fibrils that have tightly packed and proteinase K (PK)-resistant (PrP^{Res}) cores ranging from residues ~80–90 to ~231 (20–23). However, in attempting to reconstitute the PrP^C-to-PrP^D conversion under chemically defined cell-free conditions with purified recombinant PrP^C, many researchers have observed that the C-terminal domain of residues ~160–231 is much more easily converted to a PK-resistant, parallel in-register intermolecular β-sheet amyloid core than the more N-terminal residues that include prolines 102 and 105 and the CLC (12, 20, 24). Recently, we reported that the CLC strongly impedes the incorporation of residues ~90 to ~159 into a PrP^D-like amyloid core (12). Consideration of these findings in the context of in-register β-sheet models for PrP^D amyloids (25, 26) suggests that electrostatic repulsion of the cationic CLC side chains would disfavor the tight packing of these four closely spaced lysines within the amyloid core in the absence of anionic cofactors (12). Indeed, mutation of these residues to alanine or asparagine allowed more rapid and spontaneous formation of amyloid with an extended PK-resistant core. This core included epitopes with residues 90–104, as is typical of *bona fide* PrP^D (12). Thus the CLC, which surrounds prolines 102 and 105, is a critical modulator in PrP amyloid formation.

Recombinant PrP has been converted to infectious aggregates *in vitro* in the presence of cofactor additives such as 1-palmitoyl-2-oleoylphosphatidylglycerol (POPG), RNA, and phosphatidylethanolamine (27–30). Further analysis of the interaction of POPG with PrP showed that POPG associates with the central lysine cluster, and mutation of Pro-105 had a negative effect on the POPG-PrP interaction (7). These data suggest that the CLC coordinates cofactor binding to impact PrP structure.

Here, we describe the influence of pathological mutations of prolines 102 and 105 as well as the proximal lysine cluster on both spontaneous and prion-templated PrP amyloid formation. We report the effects of these mutations within the context of the full-length mature PrP sequence that is converted to amyloid in the diseased brains of humans with GSS. Moreover, we have taken care to employ conditions that are nondenaturing and at near-neutral pH. The results provide evidence that these proline and lysine residues can strongly modulate both the speed of conversion and the extent of the protease-resistant core of the resulting amyloid fibrils.

Experimental Procedures

Mutagenesis—As per the manufacturer's instructions, the Agilent Technologies QuikChange kit was used to mutate Lys-101, Lys-104, Lys-106, and Lys-110 collectively to asparagine (KN mutant) as described previously (12). Pro-102 and Pro-105 were mutated to alanine or leucine residues based on either the Syrian hamster DNA sequence encoding PrP amino acids 23–231 (accession number K02234) or the plasmid sequence encoding the KN mutant (12). Mutants were constructed using QuikChange (Agilent Technologies), Q5 site-directed mutagenesis (New England Biolabs), or Cold Fusion Systems (Biosciences) as per the manufacturer's instructions. Mutagenesis of mouse PrP was carried out based on accession number M13685.

Protein Expression and Purification—Recombinant WT and mutant PrP^C was purified as described previously (12, 31). In brief, pET41 vector containing hamster (accession number K02234), mouse (accession number M13685), or mutant PrP^c sequences was transformed into Rosetta (BL21DE3) *Escherichia coli* cells. Protein was expressed by autoinduction (32, 33). Inclusion bodies were collected and solubilized in 8 M guanidine HCl. Soluble protein was purified using Ni-NTA Superflow resin (Qiagen) with the AKTA pure chromatography system. Bound protein was refolded on the column with a linear gradient of 6 to 0 M guanidine HCl in 0.1 M sodium phosphate buffer, pH 8.0. Protein was eluted from the column with a linear gradient of 0–0.5 M imidazole in 0.1 M sodium phosphate buffer, pH 5.8. Purified protein was dialyzed into 10 mM sodium phosphate buffer, pH 5.8, and stored at −80 °C. Absorbance at 280 nm was used to determine protein concentration.

Real Time Quaking-induced Conversion (RT-QuIC)—RT-QuIC was carried out using conditions described previously (31). WT or mutant $rPrP^C$ at 0.1 mg/ml concentration was used as substrate in a 100-μl reaction containing 10 mM phosphate buffer, pH 7.4, 300 mM NaCl, 10 μM ThT, 10 μM EDTA. Reactions were plated in quadruplicate in a black 96-well clear flat-bottom plate (Nunc). Hamster substrates were seeded with 10^{-6} dilution of hamster normal brain homogenate or 263K-scrapie-infected brain homogenate. Mouse substrates were seeded with 10^{-4} dilution of mouse normal brain homogenate or 22L-infected brain homogenate. All reactions contained a final concentration of 0.002% SDS. Plates were sealed with a film and incubated in BMG Fluostar readers at 42 °C with cycles of 1 min double orbital shaking at 700 rpm and 1-min rest with ThT fluorescence measurements (450 ± 10 nm excitation and 480 ± 10 nm emission) every 45 min. Each curve is representative of quadruplicate wells. RT-QuIC reactions in 1.5-ml microcentrifuge tubes were 500-μl reactions comprised of the components described above. Samples were incubated on an Eppendorf Thermomixer R orbital shaker at 42 °C with cycles of 1 min of shaking at 700 rpm and 1 min of rest.

Proteinase K Digestion and Immunoblotting—RT-QuIC fibril reactions were treated with 30 μg/ml PK (unless otherwise indicated) at 37 °C for 1 h. PK digestion was stopped by incubating samples on ice with 1 mM Pefabloc (Sigma) for several minutes. Samples were diluted with an equal volume of 2× sample buffer (125 mM Tris-HCl, pH 6.8, 5% glycerol, 6 mM

EDTA, 10% SDS, 4% bromphenol blue, 48% urea, 8% β-mercaptoethanol) and boiled for 5 min. An equal volume of samples was run on 10% BisTris NuPAGE gels (Invitrogen), and protein was transferred to an Immobilon P membrane (Millipore) using the iBlot Gel Transfer System (Life Technologies, Inc.). PK-resistant species were detected using rabbit PrP antisera R20 (1:15,000; residues 218–231) or R30 (1:10,000; residues 90–104) (34, 35) and alkaline phosphatase-conjugated secondary antibody (1:5000; Jackson ImmunoResearch).

Transmission Electron Microscopy—Amyloid fibrils were visualized using negative stain. Ultrathin carbon-coated holey carbon copper grids (Ted Pella, Inc., Redding, CA) were subjected to a brief glow discharge, followed by immersion in 15–20 μl of fibril preparations and incubated for 45–60 min at room temperature. The grids were dipped into a droplet of deionized water before immersion in methylamine tungstate (Nanoprobes, Inc., Yaphank, NY) for 15 s, wicked of excess fluid, and air dried. Grids were analyzed at 80 kV using an H-7500 transmission electron microscope (Hitachi High Technologies, Dallas, TX) with a HR-100 digital camera system (Advanced Microscopy Techniques, Woburn, MA).

Fourier Transform Infrared (FTIR) Spectroscopy—RT-QuIC reactions in microcentrifuge tubes containing 120 μg of rPrP were allowed to run for 140 h. Samples were treated with 10–15 μg/ml PK for 1 h at 37 °C. PK digestion was stopped by incubating samples on ice with 1.5 mM Pefabloc SC (Sigma). Samples were pelleted by centrifugation at 20,800 × *g* at 4 °C for 1 h. The supernatant was removed and the pellet washed with at least 5 volumes of MilliQ water and repelleted by centrifugation at 20,800 × *g* at 4 °C for 30 min. This wash step was repeated a total of two times. The pellet was resuspended in MilliQ water to approximately a 50% w/v slurry. 1–2 μl of sample was pipetted onto the diamond of a PerkinElmer Life Sciences Spectrum 100 FT-IR spectrometer with a diamond attenuated total reflectance sample unit and MCT detector and dried to a film under a nitrogen stream. Background spectra were collected between each sample, and sample spectra were collected using 32 accumulations (4-cm^{-1} resolution; 0.2–1 cm/s scan speed, strong apodization). Data are represented as the second derivative calculated using nine data points with the Spectrum software (PerkinElmer Life Sciences).

Sequence Alignment and Phylogenetic Analysis—18 mammalian prion protein sequences were aligned using the MUSCLE alignment method (36), and a 10 amino acid sequence alignment containing the CLC was extracted. For the phylogenetic analysis, 20 vertebrate prion protein sequences were aligned using the MUSCLE alignment method (36), and a 20-amino acid sequence alignment containing the CLC was extracted, and phylogenetic analysis was performed using a maximum likelihood method (37). 1000 bootstrap reiterations were performed to validate the final format of the tree.

Results

Central Lysine Cluster Is Highly Conserved—Previous studies have demonstrated the importance of charge neutralization of the central lysine cluster (amino acids 101–110) in modulating PrP amyloid formation (12). Pro-102 and Pro-105 are contained within this highly conserved region (Fig. 1) (7), and Fig. 2*A* depicts the relative positions of these four lysine and two proline residues across 18 mammalian species with a range of life spans. The high degree of conservation suggests that the CLC lysine and proline residues have physiological significance. This might suggest an evolutionary selection for lysine and proline residues to protect against amyloid formation, particularly in species with relatively long life spans. To test whether sequence conservation correlated with species longevity or susceptibility to prion disease, we constructed a phylogenetic tree of a 20-amino acid region containing the CLC from 20 vertebrates (Fig. 2*B*) (37). We compared species across a broad range of life expectancies, including bank voles with life spans of less than a month in the wild. However, as shown in Fig. 2*B*, no noticeable grouping or clustering occurs within the tree relative to animal longevity or susceptibility to prion disease.

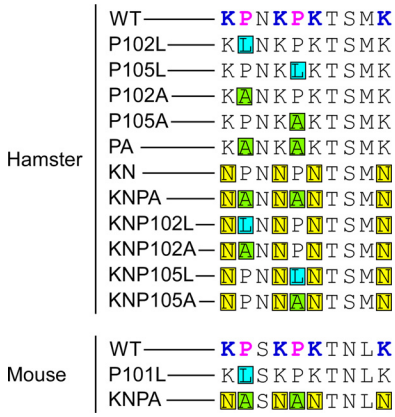

FIGURE 1. **Schematic representation of the residue substitutions in recombinant hamster and mouse PrP mutants.** Residue substitutions with the corresponding mutant PrP nomenclature are indicated in the *colored boxes*; with *blue* depicting a leucine, *green* an alanine, and *yellow* an asparagine substitution.

P102L Spontaneously Forms Amyloid in the Absence of Denaturants—To test the influence of Pro-102 and Pro-105 on PrP amyloidogenesis, we mutated these residues to either leucine or alanine residues (Fig. 1) and monitored PrP amyloid formation at pH 7.4 and 300 mM NaCl using intermittent shaking and the amyloid-sensitive fluorescent dye, ThT. The hamster PrP background was used unless otherwise denoted. These reaction conditions were like those previously described as RT-QuIC (31). The proline mutations did not affect the kinetics of scrapie brain homogenate (ScBH)-seeded amyloid formation (Fig. 3, *A* and *B*). However, mutation of Pro-102 to leucine (P102L) expedited spontaneous formation of amyloid in the presence of scrapie-free normal brain homogenate (NBH). Spontaneous conversion of the P102L mutant to ThT-positive amyloid occurred after a lag phase of ~30 h. The P105A mutant also spontaneously formed amyloid, albeit in only ~25% of replicate reactions with much longer lag times (Fig. 3*B*, *top panel*). As previous studies on the pathological P102L mutation focused primarily on mouse models (P101L), we also investigated whether the mouse P101L mutant behaved similarly to hamster P102L rPrP. Indeed, moP101L readily formed amyloid both with and without scrapie-seeding in RT-QuIC reactions (Fig. 3*C*).

We used Western blot analysis of PK-treated RT-QuIC conversion products to compare the amyloid cores that could be

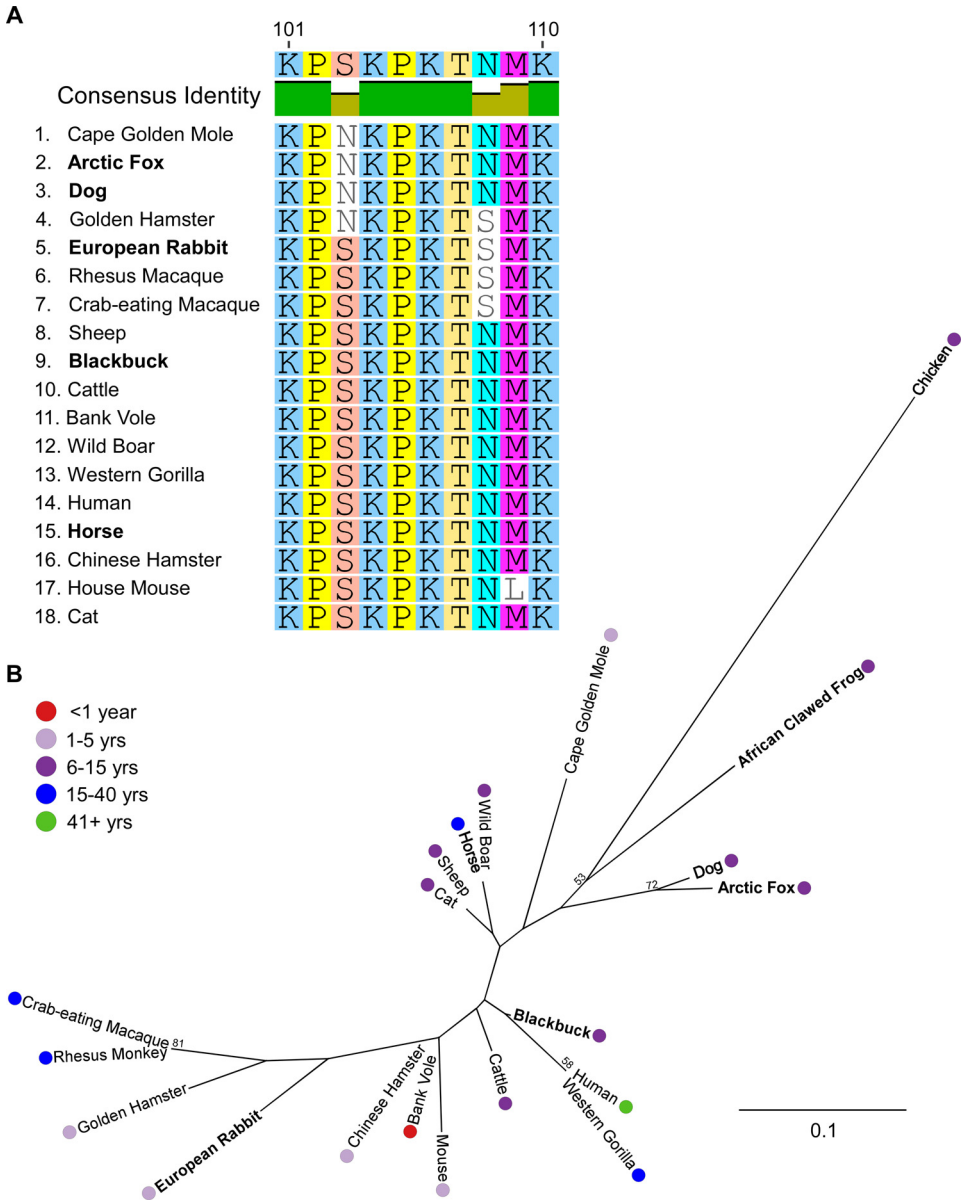

FIGURE 2. *A,* sequence alignment of the CLC (amino acids 101–110 based on the human PrP sequence) indicates a high degree of conservation between 18 mammalian species. *B,* maximum likelihood phylogenetic analysis of a 20-amino acid segment inclusive of the CLC region. The phylogenetic tree represents the relationship between the CLC regions of the 20 different vertebrates. Typical life span is indicated with a colored *dot* besides the species name. Species with reduced susceptibility to prion disease are indicated in *bold*. Bootstrap values greater than 50% are shown at the *branch points* to indicate likelihood of branching pattern. The *scale bar* for branch length represents the number of base substitutions per site analyzed. Grouping or clustering of groups according to lifespan (as indicated by the *colored dots*) would indicate a relationship of the CLC with longevity. However, given the wide disbursement of species of similar life spans, no obvious relationship between the 20-amino acid segment containing the CLC with longevity or susceptibility to prion disease was apparent.

generated using the mutant rPrPs. Because it was difficult to recover RT-QuIC products from multiwell plates due to tight adherence of the reaction products to the plastic, we performed shaken reactions under identical buffer conditions in less adherent microcentrifuge tubes. These reactions were allowed to proceed until amyloid was formed in all cases, even without scrapie-seeding. Spontaneously formed and scrapie-seeded wild-type and mutant rPrPs each produced C-terminal PK-resistant core fragments of ~10–14 kDa recognized by an antiserum recognizing C-terminal residues 218–231 (R20) (Fig. 4). The scrapie-seeded conversion of P102L rPrP also promoted an N-terminal extension of the PK-resistant core to ~17–19 kDa (Fig. 4*A*). This fragment was recognized by antiserum R30, indicating N-terminal extension into the epitope of residues 90–104. This 17–19-kDa amyloid core was sometimes (Fig. 4*A*) formed in the presence of normal brain homogenate as well. Similar extensions of the amyloid core to ~17–19 kDa were observed with P105L, P102A, and P105A mutant rPrPs, but usually to a lesser extent than we saw with P102L (Fig. 4, *A* and *B*). Additionally, P102L and P102A mutant rPrPs formed an extended amyloid core of ~19 kDa that was 2 kDa larger than the ~17-kDa amyloid core formed with P105L and P105A mutant rPrPs (Fig. 4, *A* and *B*). Analysis of both normal brain homogenate and scrapie-seeded amyloid formed with the mouse P101L rPrP mutant under RT-QuIC conditions indicated PK-resistant amyloid cores of 10–14 and 19-kDa (Fig.

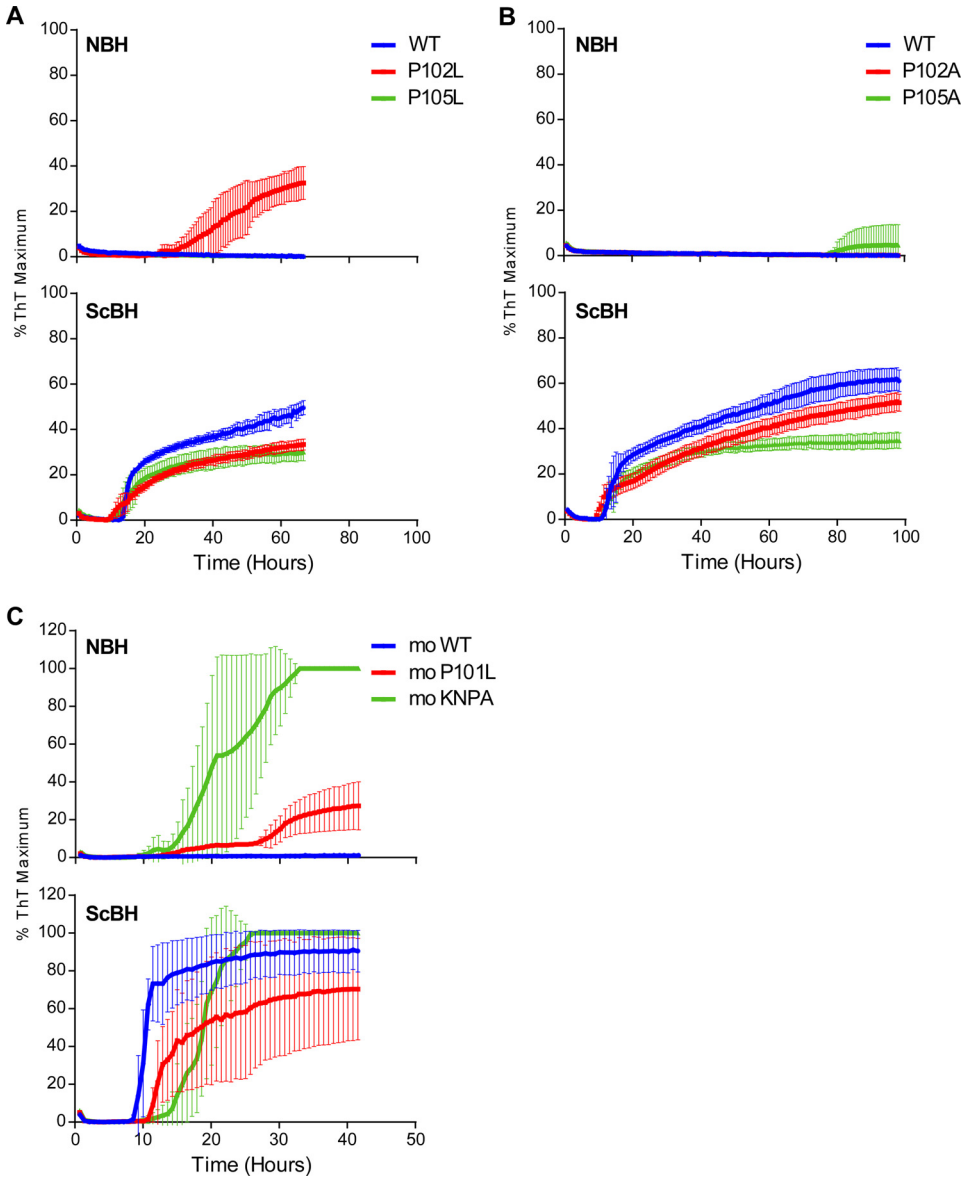

FIGURE 3. **P102L mutations in 23–231 rPrP promoted amyloid formation without scrapie seeding.** RT-QuIC reactions were used to monitor amyloid formation over time using ThT fluorescence (mean ± S.D. of four replicate wells) as a read-out. Hamster rPrP containing mutations of Pro-102 or Pro-105 to leucine (*A*) or alanine (*B*) all formed amyloid with scrapie seeding (*bottom panel*). Only P102L readily formed amyloid spontaneously, *i.e.* in the presence of uninfected normal brain homogenate (*A, top panel*). Data are representative of at least three independent experiments. *C,* kinetics of mouse wild type (*WT*), P101L, and KNPA PrP amyloid formation were monitored using the RT-QuIC. WT, P101L, and KNPA rPrP all form amyloid with scrapie seeding (*bottom panel*), whereas P101L and KNPA spontaneously form amyloid (*top panel*). Data are representative of two independent experiments. *NBH,* normal brain homogenate; *ScBH,* scrapie brain homogenate.

4*C*), similar to those observed with hamster P102L rPrP (Fig. 4*A*). Altogether, the data indicated that mutation of either Pro-102 or Pro-105 promoted extension of the PK-resistant amyloid core to span between epitopes within residues 90–104 and 218–231, which is similar to the core frequently observed with scrapie-associated PrP^D (22, 23, 34).

FTIR spectroscopy indicated that hamster wild-type and P102L rPrP amyloid formed in microcentrifuge tubes absorbed strongly in the β-sheet region (~1620–1636 cm^{-1}) (Fig. 5). As reported previously, scrapie-seeded wild-type amyloid tended to show a diminished 1620-cm^{-1} band relative to the 1634-cm^{-1} band when compared with wild-type amyloid formed in the presence of normal brain homogenate (Fig. 5*A*). In contrast, the prion seeding did not appear to influence P102L amyloid secondary structure as both normal brain homogenate and scrapie-seeded P102L amyloid gave similar spectra (Fig. 5*B*). However, the relative intensities of the P102L 1634-, 1626-, and 1620-cm^{-1} bands varied significantly between individual reactions. This, and the multiple PK-resistant amyloid cores observed by Western blot (Fig. 4*A*), suggested that multiple conformers were generated in varying proportions in these reactions.

Rapid Scrapie-independent Amyloid Formation with Mutation of CLC Lysine and Proline Residues—Having seen that mutation of either the proline or lysine residues within the CLC influenced the propensity for PrP amyloid formation (see above and Ref. 12), we then investigated the combined effects of such mutations. Mutations of both Pro-102 and Pro-105 to alanine

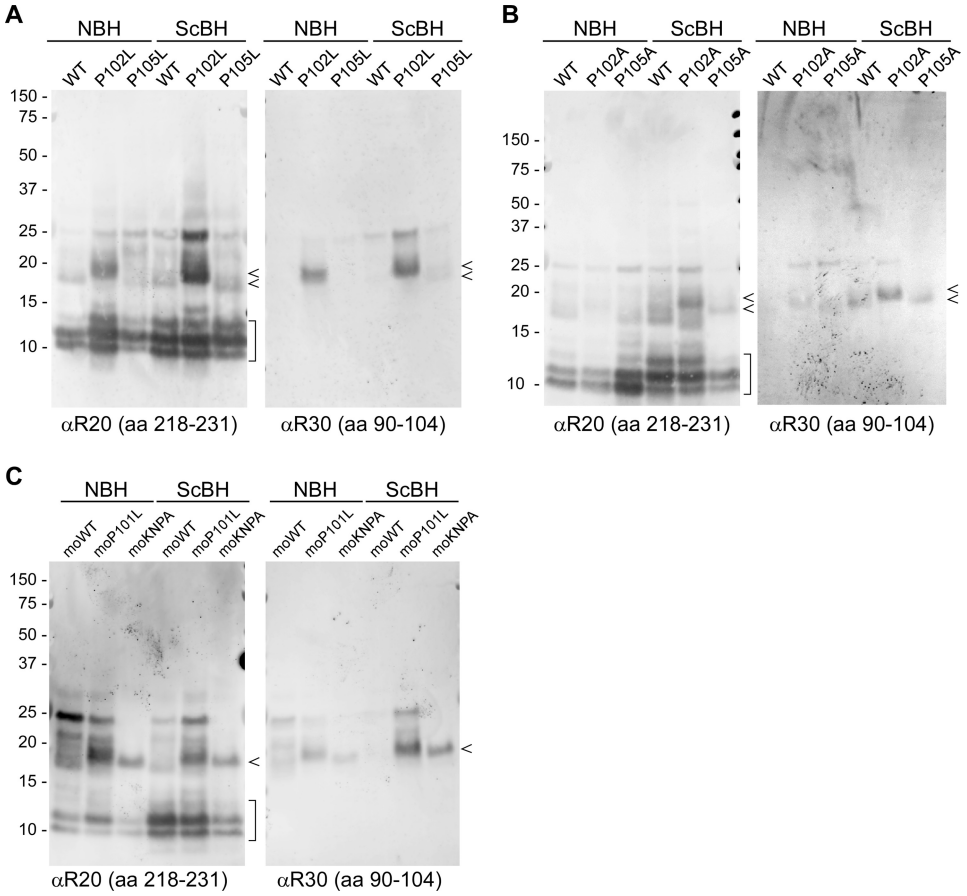

FIGURE 4. **PK digestion and Western blot analysis of RT-QuIC products indicated that proline substitution in hamster and mouse PrP promoted N-terminal extension of the amyloid core.** In scrapie-seeded reactions, both Pro-102 and Pro-105 mutated to leucine (*A*) or alanine (*B*) in hamster PrP allowed formation of an extended amyloid core (*arrowheads*) recognized by antisera directed to residues 218–231 (*R20*) and residues 90–104 (*R30*) in addition to the 10–14-kDa cores (*bracket*) recognized by R20 antisera. Figures are representative of three or more independent experiments. *C,* both normal brain homogenate and scrapie-seeded mouse P101L and mouse KNPA reactions demonstrate N-terminal extension of the amyloid core to ~17–19 kDa (*arrowhead*), recognized by R20 and R30 antisera in addition to the 10–14-kDa amyloid cores (*bracket*). Results are representative of two independent experiments. *NBH,* normal brain homogenate; *ScBH,* scrapie brain homogenate. *aa*, amino acids.

residues (PA) in hamster PrP did not impact the kinetics of scrapie-seeded amyloid formation relative to that of wild-type rPrP (Fig. 6*A*). However, combined mutations of both prolines 102 and 105 to alanines as well as the four CLC lysines to asparagines (KNPA) resulted in more rapid amyloid formation. In addition, there was no longer a discernable difference in the lag phase between normal brain homogenate and scrapie-seeded KNPA amyloid formation (Fig. 6*A*). For unknown reasons, KNPA amyloid formation reproducibly had biphasic kinetics, with a rapid increase in ThT fluorescence, a brief plateau of ~10 h, followed by a second increase in ThT fluorescence. Western blot analysis of these RT-QuIC products revealed both the normal brain homogenate and scrapie-seeded formation of an ~17-kDa PK-resistant amyloid core recognized by antisera to residues 90–104 and 218–231 in addition to the C-terminal ~10–14-kDa PK-resistant amyloid cores recognized by an antiserum to 218–231 (Fig. 6*B*). Similar results were obtained using mouse KNPA rPrP with both normal brain homogenate and scrapie-seeded amyloid formation showing a comparable lag phase (Fig. 3*C*) and formation of the extended ~17-kDa PK-resistant amyloid core in addition to the C-terminal ~10–14-kDa PK-resistant amyloid cores recognized by antisera to 218–231 (Fig. 4*C*). Thus, substitution of the CLC lysine and proline residues promoted self-nucleating amyloid formation with kinetics similar to scrapie-seeded reactions.

FTIR analyses of KNPA amyloid showed peaks that absorbed in the β-sheet region (Fig. 6*C*). Similar to the P102L amyloid, there was no systematic differences between KNPA amyloid formed with or without a prion seed. KNPA amyloid also had 1634-, 1626-, and 1620-cm^{-1} bands reminiscent of the 263K prion seed, albeit with somewhat varied relative intensities between experiments (Fig. 6*C*), providing evidence of conformational heterogeneity between the products of individual reactions.

As Pro-102 and Pro-105 are mutated individually in human prion disease, we also explored the role of single proline mutations in the context of a charge-neutralized lysine cluster. Similarly to the KNPA mutant, mutations of Pro-102 or Pro-105 to leucine or alanine individually on the KN background resulted in rapid spontaneous amyloid formation with lag phases similar to the corresponding scrapie-seeded amyloid formation (Fig. 7, *A* and *B*). Western blot analyses showed that mutation of individual prolines together with the CLC lysine mutations to asparagines allowed formation of the ~10–14 kDa and the N-terminally extended 17-kDa amyloid cores under both normal brain homogenate and scrapie-seeded conditions (Fig. 7, *C*

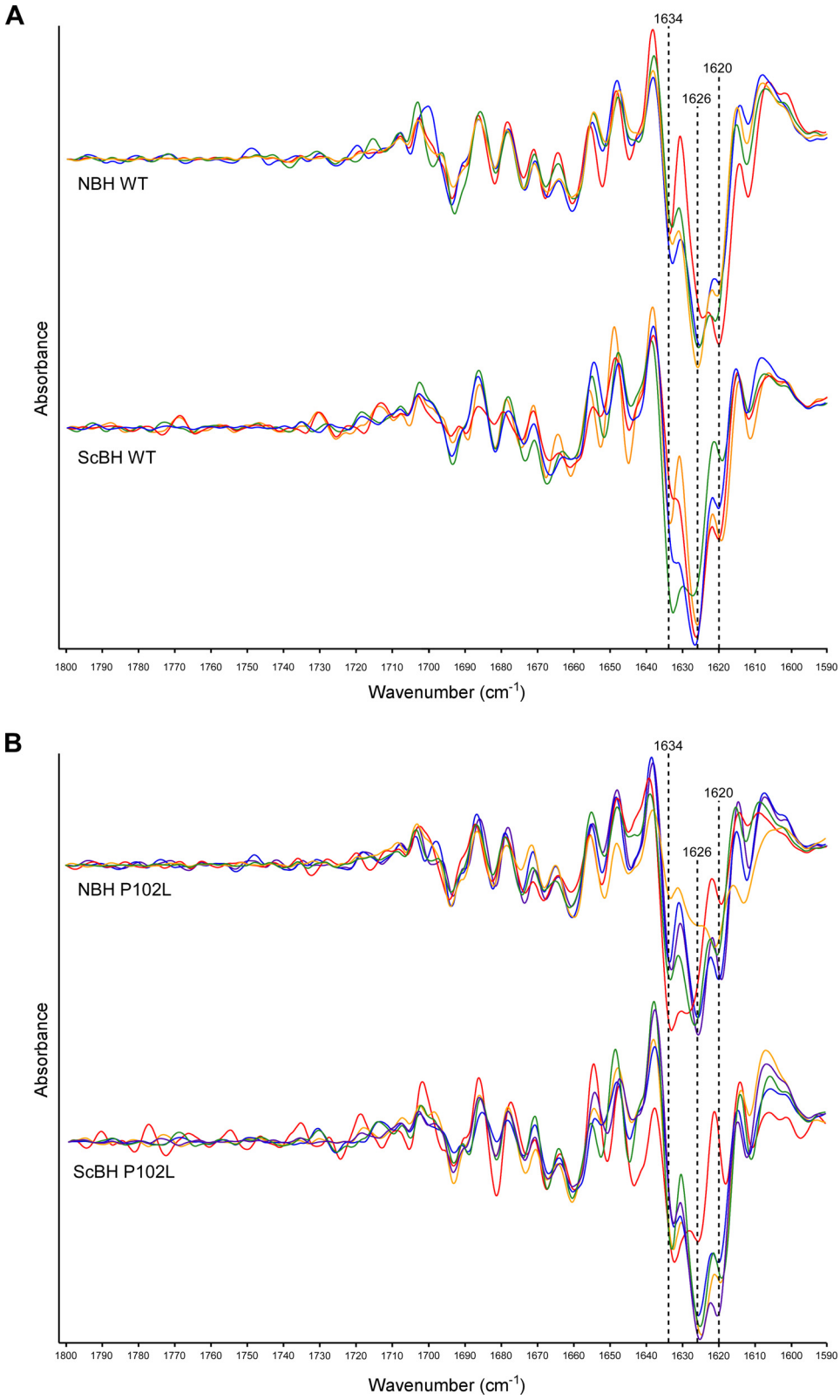

FIGURE 5. **Normal brain homogenate and scrapie-seeded P102L amyloid showed similar β-sheet secondary structure by FTIR analyses.** *A,* scrapie-seeded WT amyloid had a diminished 1620-cm^{-1} peak relative to the 1634-cm^{-1} peak, and WT amyloid formed in the presence of normal brain homogenate had a more prevalent 1620-cm^{-1} peak. *B,* normal brain homogenate and scrapie-seeded P102L showed similar spectra, albeit with some experimental variation in the intensities of the 1620- and 1634-cm^{-1} peaks. Each *curve* represents products of independent fibril preparations. *NBH,* normal brain homogenate; *ScBH,* scrapie brain homogenate.

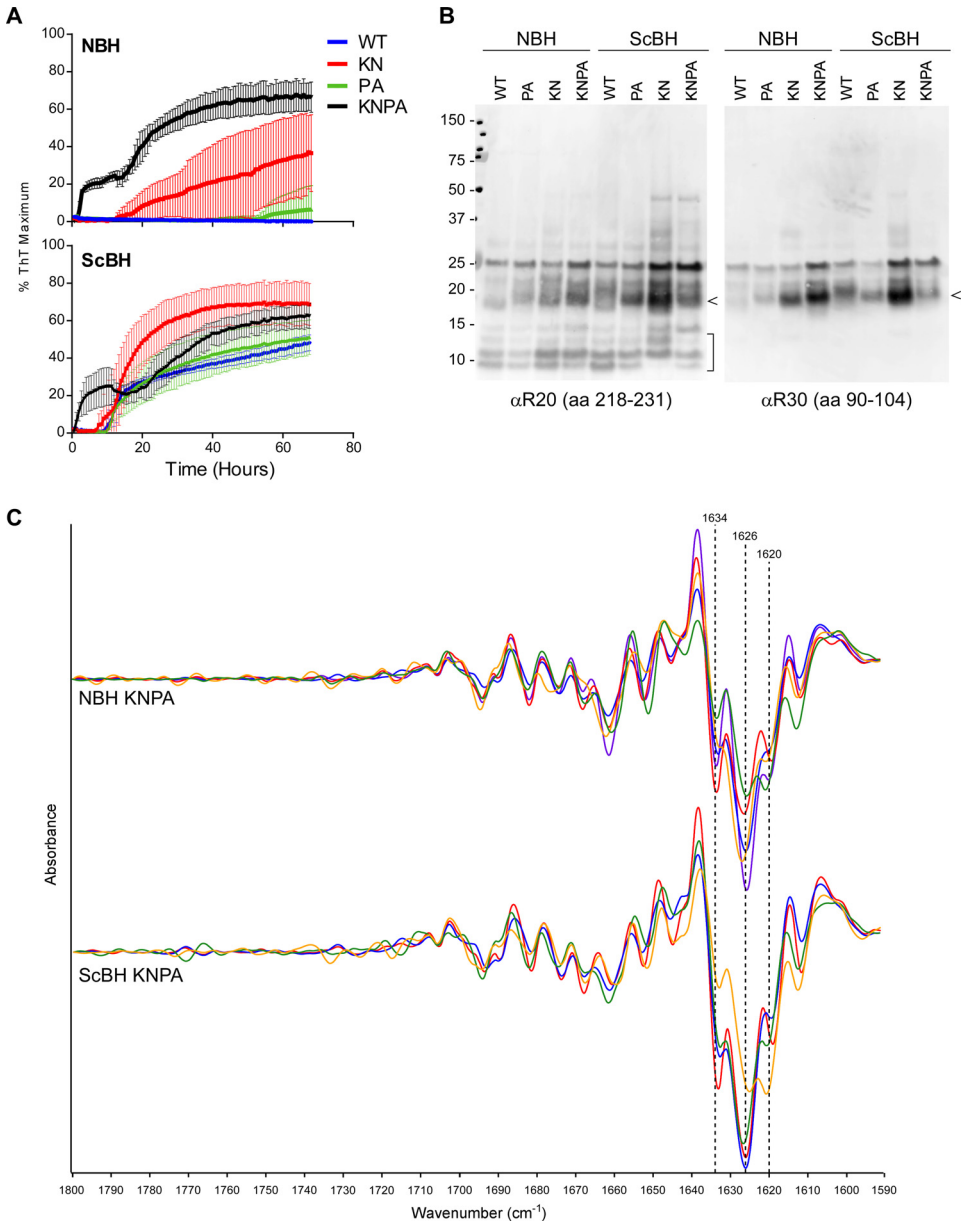

FIGURE 6. **Mutation of lysine and proline residues within the central lysine cluster accelerates seeding-independent kinetics of PrP amyloid formation.** *A,* RT-QuIC was used to analyze the kinetics of amyloid formation of hamster WT, KN, PA, and KNPA rPrP. Scrapie-seeded PA shows similar kinetics to WT substrate (*bottom panel*), and KNPA forms amyloid with rapid kinetics with similar lag phases between normal brain homogenate (*top panel*) and scrapie-seeded (*bottom panel*) reactions (compare NBH KNPA to ScBH KNPA). *B,* Western blot analysis of PK-digested RT-QuIC products using antisera directed to residues 218–231 (R20) and residues 90–104 (R30). Extension of the amyloid core is visible in KN, PA, and KNPA substrates (compare 17-kDa bands (*arrowheads*) to 10–14-kDa bands (*bracket*)). Figures are representative of three independent experiments. *C,* normal brain homogenate and scrapie-seeded KNPA showed similar 1634-, 1626-, and 1620-cm^{-1} bands in the β-sheet region by FTIR analysis. *aa*, amino acids.

and *D*). Thus, mutation of a single proline residue within a charge-neutralized CLC is sufficient to accelerate spontaneous amyloidogenesis and negate the need for prion templating to allow N-terminal extension of the amyloid core. Furthermore, FTIR analyses indicated that like KNPA, KNP102L amyloid absorbed strongly in the β-sheet region with similar 1634-, 1626-, and 1620-cm^{-1} bands with and without prion seeding (Fig. 7*E*).

Ultrastructural Analysis—Negatively stained products of various RT-QuIC reactions were analyzed by transmission electron microscopy (Fig. 8). Scrapie-seeded RT-QuIC reactions were used to seed subsequent RT-QuIC reactions that were incubated with slower shaking speeds to prevent fibril clumping and shearing. The P102L, KNP102L, and KNPA mutant rPrPs examined all formed fibrillar structures typically 6–16 nm in width. Although the fibrillar structures were somewhat variable, KNP102L and KNPA typically formed shorter fibrils than P102L.

Mutation of CLC Lysine and Proline Residues Enhanced the Overall PK Resistance of the Amyloid Cores—To further compare the characteristics of the amyloid products, we digested scrapie-seeded RT-QuIC conversion products with increasing amounts of PK (Fig. 9). P102L formed ~10–14-kDa cores and an extended 17–19-kDa amyloid core resistant to 30 μg/ml PK

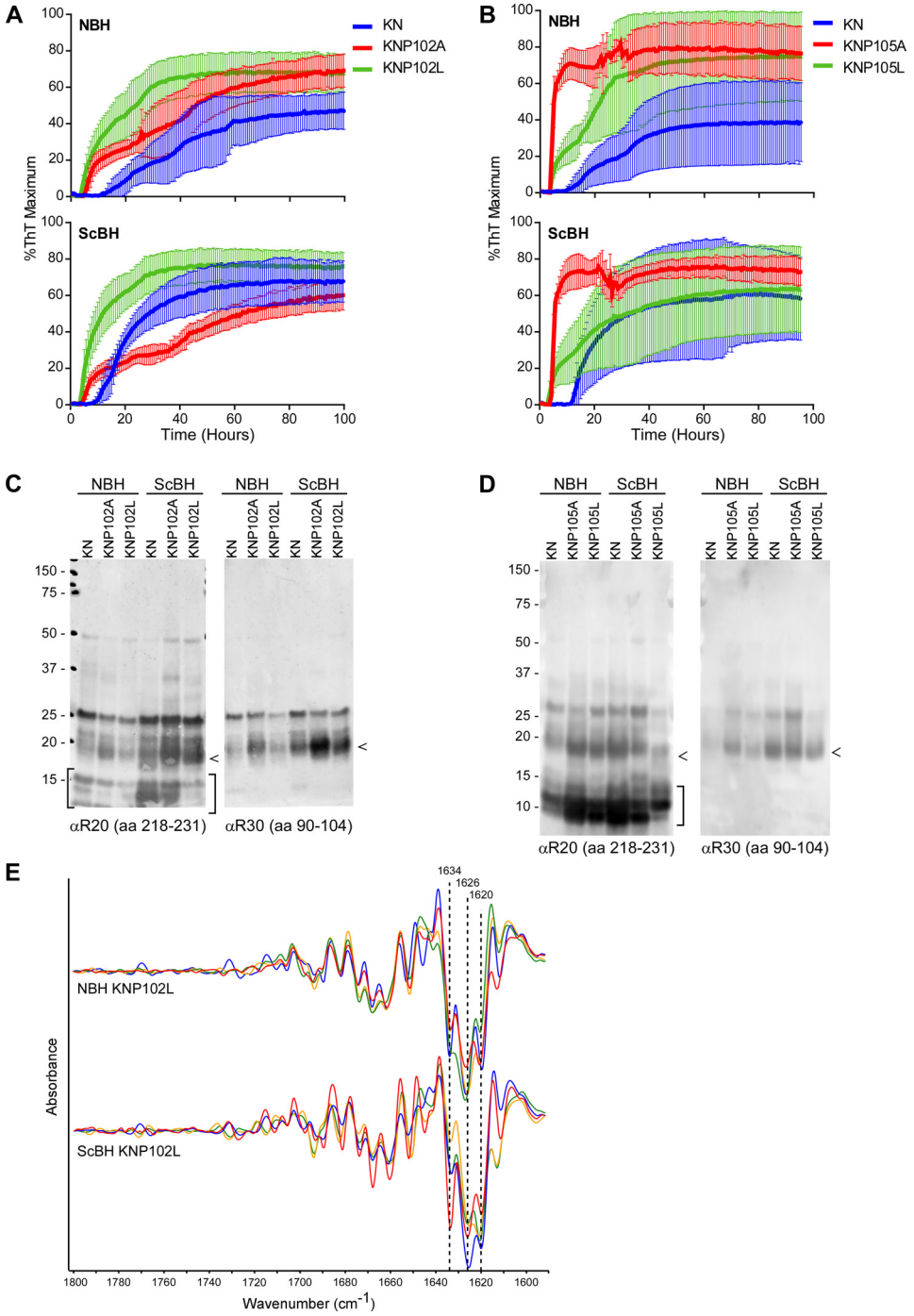

FIGURE 7. **Mutation of either Pro-102 or Pro-105 in conjunction with CLC charge neutralization is sufficient to accelerate template-independent kinetics of amyloid formation.** RT-QuIC analysis indicated mutation of Pro-102 (*A*) or Pro-105 (*B*) to leucine or alanine in conjunction with mutation of the four lysine residues to asparagine accelerates template independent kinetics of amyloid formation (compare normal brain homogenate (*NBH*, *top panel*) and scrapie-seeded (*ScBH*, *bottom panel*) reactions). Figures are representative of the mean ± S.D. of four replicate wells in two independent experiments. *C* and *D*, Western blot analysis of the PK-digested RT-QuIC conversion products shows N-terminally extended mutant PrP amyloid cores (*arrowheads*) that are recognized by both R20 and R30 antisera in addition to the 10–14-kDa amyloid cores (*bracket*). *E*, KNP102L amyloid formed with (*ScBH*) or without (*NBH*) scrapie seeding showed similar FTIR spectra with predominant 1634-, 1626-, and 1620-cm^{-1} bands in the β-sheet region. *NBH*, normal brain homogenate; *ScBH*, scrapie brain homogenate. *aa*, amino acids.

(Fig. 9, *C* and *D*). The KNPA and KNP102L mutants formed ~10–14-kDa and robust 17-kDa cores resistant to PK concentrations of >40 μg/ml (Fig. 9, *A–D*). Thus, although mutation of individual proline or lysine residues allowed formation of an extended PK-resistant core, mutation of both sets of residues together increased the PK-resistance of the N-terminally extended amyloid core.

Mutant Amyloids Seed Amyloid Formation of Wild-type rPrP^{Sen} Substrate—After seeing that mutation of proline and lysine residues within the CLC region promoted PrP amyloidogenesis, we tested whether the mutant conversion products could in turn seed further amyloid formation of wild-type PrP. Using RT-QuIC conditions, we seeded reactions with 10^{-3} dilutions of the mutant amyloid (Fig. 10). Both spontaneously

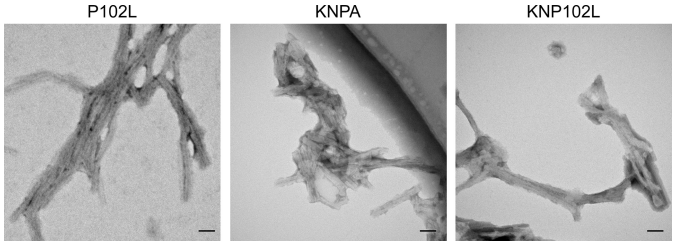

FIGURE 8. **Negative stain electron micrographs of P102L, KNPA, and KNP102L mutant rPrP amyloids formed with scrapie seeding indicate that these mutants are able to form fibrillar structures.** *Scale bar,* 50 nm.

formed and scrapie-seeded KNPA, P102L, and KNP102L amyloid were able to seed conversion of wild-type *rPrP*^{Sen}.

Discussion

The fact that mutations of Pro-102 and Pro-105 are linked to PrP^{D} accumulation and devastating human prion disease (38, 39) suggests that these prolines protect against the pathologic misfolding of PrP^{C}. Our current demonstration that substitution of these proline residues with the disease-linked leucines accelerates PrP amyloid formation of N-terminally extended PK-resistant amyloid cores reminiscent of PrP^{D} is consistent with this possibility. These proline residues, as well as the surrounding cluster of four lysines, are well conserved among mammals, suggesting that the sequence within this CLC region is of physiological significance. Although the sequence of this region may be important in the enigmatic function of PrP^{C}, accumulating evidence is consistent with the possibility that the amino acid composition of the CLC may also be evolutionarily selected to impede the accumulation of neurotoxic and/or infectious aggregates. Indeed, substitution of both proline and lysine residues within the CLC significantly accelerated the spontaneous and scrapie-seeded conversion of full-length PrP to amyloid. In fact, altering the lysine and proline composition of the CLC allowed spontaneous PrP^{D}-like amyloid formation with identical lag phases to scrapie-seeded amyloid formation, implying that the CLC proline and lysine residues can impede PrP conversion to pathological forms.

Without knowing the conformations of either PrP^{C} or PrP^{D} in the CLC region, it is difficult to ascertain the detailed structural reasons for the effects on PrP amyloid formation with substitution of the associated proline and lysine residues. In previous studies with a C-terminally truncated fragment of PrP, PrP(23–144), P102L and P105L did not alter PrP amyloidogenicity (40). However, the amyloid formation of mutant PrP(23–144) molecules was measured only after seeding with synthetic preformed fibrils (40). Here, we observed that mutation of Pro-102 to a leucine within full-length PrP expedited spontaneous amyloid formation. This kinetic effect indicated that the P102L mutation reduced a rate-limiting energy barrier in the conversion to amyloid fibrils. This effect was further enhanced with additional charge neutralization of the lysine cluster. In unseeded nucleated polymerization reactions, the rate-limiting event is usually nucleation rather than the elongation of fibrils (41). However, our observation that the PK-resistant cores of the final mutant and wild-type amyloids differed indicated that the proline and lysine mutations affected the structure of the products, as well as the substrates and/or transition states, of the overall fibrillization reaction. The mechanistic reason for these effects is unclear, but the replacement of a proline residue with a leucine would add a bulkier hydrophobic side chain and relieve the backbone torsional conformational constraints imposed by the cyclic nature of prolines. For example, proline residues tend to disrupt β-strands (42). The replacement of a proline with a leucine should not in itself eliminate a PK cleavage site in the primary sequence because PK prefers to cut after aliphatic and aromatic residues. Thus, it seems likely that the primary effect of the leucine residues was conformational. At the same time, we note that mutations of Pro-105 to serine or threonine have also been linked to prion disease in humans (38, 39). These latter substitutions at Pro-105 would increase side chain hydrogen-bonding capacity rather than hydrophobicity. Charge neutralization of the surrounding lysine residues likely eliminates local electrostatic repulsion that could presumably impede PrP amyloid formation in the absence of a charge compensatory cofactor. Thus, multiple types of perturbations in the CLC region can promote the pathological aggregation of PrP.

P102L and P102A mutations allowed formation of an extended ~19-kDa amyloid core that was ~2 kDa larger than the ~17-kDa core formed with similar mutations of Pro-105 (Fig. 4), suggesting the local rPrP^{Res} structure differed depending on which proline residue was mutated. This additional ~2-kDa shift was no longer readily visible when proline mutations were combined with charge neutralization of the lysine cluster. It is possible that the local structure dictated by the proline residues is dependent on the lysine composition within the CLC.

Cofactors such as POPG, RNA, and phosphatidylethanolamine are known to support the formation of infectious PrP *in vitro* (27–30). POPG can bind to the CLC and adjacent hydrophobic domain, and indeed, it has been suggested that Pro-102 and Pro-105 might influence the arrangement of the surrounding cationic residues to affect polyanionic cofactor-binding sites (7). However, charge neutralization of the CLC lysine residues did not impact the POPG-PrP interaction under physiological salt conditions (7), indicating that the binding of phospholipids is not largely dependent upon electrostatic interactions with the CLC. P*XX*P motifs, like that found in the CLC, are often found in protein-binding sites and can assume a polyproline II helical secondary structure. Perhaps disruption of such secondary structure through mutation of the CLC promotes inclusion of the N-proximal region in the amyloid core in the absence of cofactors.

The P102L or P105L mutants have a reduced ability to convert to an infectious PK-resistant conformation in the presence of a lipid (7), yet under the conditions reported here, proline mutation increased the propensity for amyloid formation. The reason for this apparent discrepancy is not clear, but we note that the previous study measured for conversion after only a 1-h incubation, which might not have been long enough for detectable conversion, especially considering the ~30-h lag phase for P102L amyloid formation that we have observed here. Additionally, P102L and P105L mutants might not require a cofactor for *in vitro* conversion, as is the case with other familial PrP mutations (43). Thus, co-incubation of such mutants, either with or without cofactors, in the absence of shaking, sonication,

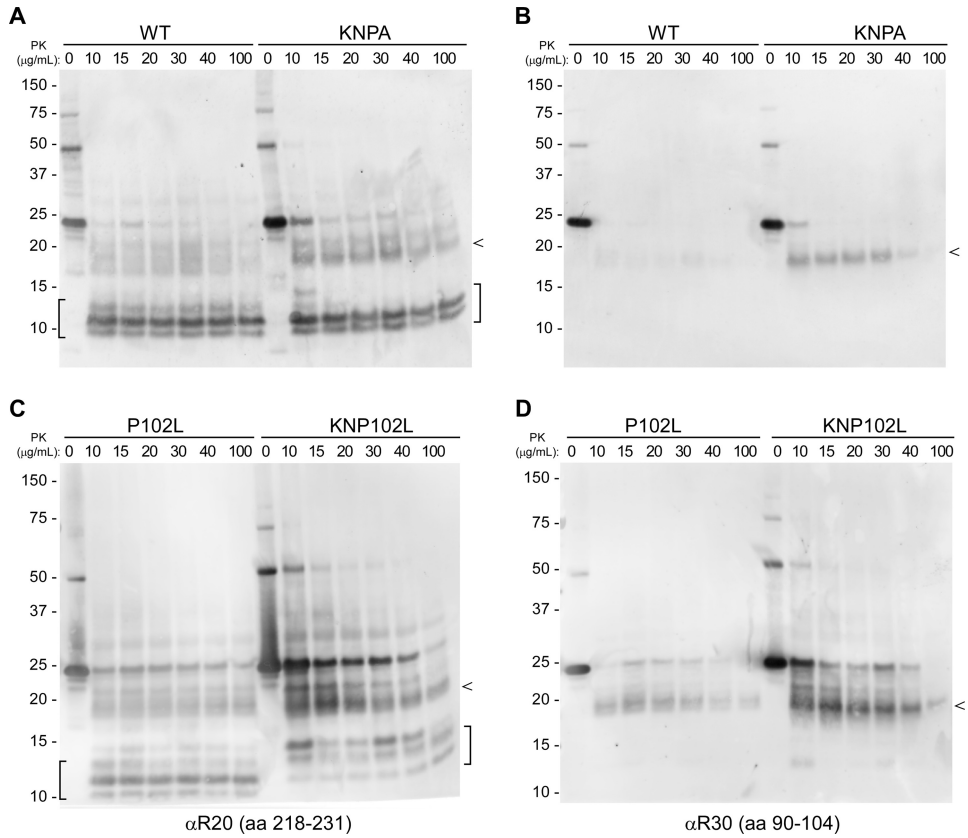

FIGURE 9. **PK digestion of proline and lysine mutant PrP amyloids.** Scrapie-seeded amyloid formed in the RT-QuIC was digested using increasing amounts of PK and analyzed by Western blot using R20 (epitope 218–231) and R30 (epitope 90–104) antisera. Immunoblots show PK-resistant amyloid cores of 10–14 kDa (*brackets*) in all rPrPs. Mutation of lysine and/or proline residues allows PK-resistant N-terminal extension of the amyloid core as indicated by the band at ~17–19 kDa (*arrowheads*) that is recognized by both R20 (*A, C*) and R30 (*B, D*) antisera. *aa,* amino acids.

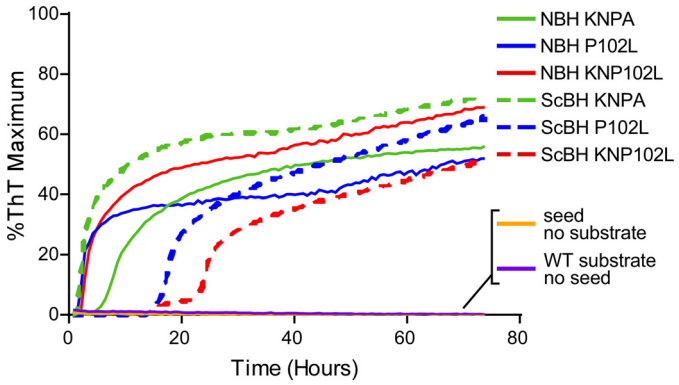

FIGURE 10. **Amyloid fibrils formed from proline and lysine mutants seed wild-type PrP amyloid formation.** Fibrils formed from normal brain homogenate and scrapie-seeded (*ScBH*) RT-QuIC reactions with mutant substrates P102L, KNP102L, and KNPA were used to seed conversion of WT substrate in the RT-QuIC.

or extended incubation may not have been sufficient to induce amyloid formation in the previously reported experiments.

In considering our results in the context of the proposed parallel in-register intermolecular β-sheet architectures (26), we note that the incorporation of the CLC region into tightly packed solvent-excluding amyloid, faces apparent obstacles as follows: electrostatic repulsion between positively charged lysine side chains and the inclusion of two proline residues, which normally disrupt β-sheets. The mutant PrPs examined here were designed to help overcome these obstacles, and our findings that they more readily form amyloids with extended PK-resistant cores are consistent with this modeling. Inclusion of prolines in an in-register β-sheet structure would presumably induce kinks or bends in the peptide backbone. As we have postulated previously, variations in the turns and bends needed to pack an in-register β-sheet PrP monomer within a fibrillar cross-section could be the basis of distinct prion strain templates (26). It seems plausible that the proline residues could influence the placement of such turns.

We initially hypothesized that animals with increased longevity or ages of fertility (*e.g.* humans) would have increased evolutionary pressure to select for proline and lysine residues to help prevent PrP^C conversion to PrP^D, although this may be less important in animals with shorter life spans or fertility spans. However, although the degree of conservation suggests an important physiological role of the CLC, it is not apparent that evolutionary pressures on the CLC correlate to longevity (Fig. 2*B*). Thus, sequence conservation in this region of PrP might be related to its ill-defined physiological structure and function, independent of influences on pathological amyloid formation. Still, increasing evidence indicates that Pro-102 and Pro-105 can impede PrP misfolding, which is consistent with reports indicating that inclusion or modulation of proline residues can also influence the formation of various other amyloids (14–17). Thus, Pro-102 and Pro-105 might act as modulatory proline switches in PrP misfolding, similar to proline switches in other amyloid-forming proteins. Without knowing the detailed con-

formation(s) of PrP^{Sc}, we cannot say whether these prolines are in the *cis* or *trans* conformation within PrP^{Sc}. In PrP^{C}, these prolines are within a highly flexible region as has been indicated by numerous NMR studies (44–46). Using combined sequence and NMR chemical shift information from a human recombinant 90–231 PrP molecule (44), the Promega program (47) predicts that for Pro-102 and Pro-105 the Xaa-Pro peptide bond conformations are very unlikely to be in a *cis* form.[3] Whether a proline switch from *trans* to *cis* is required for PrP^{C} conversion to PrP^{Sc} remains to be determined.

The P101L(89–143) peptide was only able to induce TSE disease when inoculated into P101L transgenic animals and did not cause detectable clinical disease in wild-type animals (6). Although the mutant PrP amyloids described above are able to seed amyloid formation of wild-type rPrP in the RT-QuIC assay (Fig. 10), it remains to be seen whether substitution of the CLC lysine and proline residues allows PrP conversion into its *bona fide* infectious form *in vivo*. In any case, our current findings highlight the proline and lysine residues within the CLC as critical structural modulators of PrP amyloid formation.

Author Contributions—A. K., B. R. G., and B. C. conceived the study. A. K. designed and A. K. and K. J. A. conducted and analyzed experiments. L. D. R. purified protein constructs. C. M. conducted phylogenetic analysis. D. W. D. took TEM images. A. K. and B. C. wrote the manuscript.

Acknowledgments—We thank Drs. Suzette Priola, Roger Moore, and James Carroll for critical evaluation of the manuscript and Anita Mora and Austin Athman for graphics assistance. We thank Prof. Brian Sykes, University of Alberta, for obtaining predictions of the cis-trans conformations of Pro-102 and Pro-105 for us.

References

1. Ironside, J. W., Ghetti, B., Head, M. W., Piccardo P., and Will, R. G. (2008) in *Greenfield's Neuropathology* (Love, S., Louis, D., and Ellison, D. W., eds) pp. 1197–1274, Hodder Harnold, London
2. Ghetti, B., Bugiani, O., Tagliavini, F., and Piccardo, P. (2003) in *Neurodegeneration: The Molecular Pathology of Dementia and Movement Disorders* (DW, D., ed) pp. 318–325, ISN Neuropath Press, Basel
3. Hsiao, K. K., Scott, M., Foster, D., Groth, D. F., DeArmond, S. J., and Prusiner, S. B. (1990) Spontaneous neurodegeneration in transgenic mice with mutant prion protein. *Science* **250,** 1587–1590
4. Hsiao, K. K., Groth, D., Scott, M., Yang, S. L., Serban, H., Rapp, D., Foster, D., Torchia, M., Dearmond, S. J., and Prusiner, S. B. (1994) Serial transmission in rodents of neurodegeneration from transgenic mice expressing mutant prion protein. *Proc. Natl. Acad. Sci. U.S.A.* **91,** 9126–9130
5. Manson, J. C., Jamieson, E., Baybutt, H., Tuzi, N. L., Barron, R., McConnell, I., Somerville, R., Ironside, J., Will, R., Sy, M. S., Melton, D. W., Hope, J., and Bostock, C. (1999) A single amino acid alteration (101L) introduced into murine PrP dramatically alters incubation time of transmissible spongiform encephalopathy. *EMBO J.* **18,** 6855–6864
6. Kaneko, K., Ball, H. L., Wille, H., Zhang, H., Groth, D., Torchia, M., Tremblay, P., Safar, J., Prusiner, S. B., DeArmond, S. J., Baldwin, M. A., and Cohen, F. E. (2000) A synthetic peptide initiates Gerstmann-Straussler-Scheinker (GSS) disease in transgenic mice. *J. Mol. Biol.* **295,** 997–1007
7. Wang, F., Yin, S., Wang, X., Zha, L., Sy, M. S., and Ma, J. (2010) Role of the highly conserved middle region of prion protein (PrP) in PrP-lipid interaction. *Biochemistry* **49,** 8169–8176
8. Inouye, H., Bond, J., Baldwin, M. A., Ball, H. L., Prusiner, S. B., and Kirschner, D. A. (2000) Structural changes in a hydrophobic domain of the prion protein induced by hydration and by Ala → Val and Pro → Leu substitutions. *J. Mol. Biol.* **300,** 1283–1296
9. Wan, W., Wille, H., Stöhr, J., Kendall, A., Bian, W., McDonald, M., Tiggelaar, S., Watts, J. C., Prusiner, S. B., and Stubbs, G. (2015) Structural studies of truncated forms of the prion protein PrP. *Biophys. J.* **108,** 1548–1554
10. Cappai, R., Stewart, L., Jobling, M. F., Thyer, J. M., White, A. R., Beyreuther, K., Collins, S. J., Masters, C. L., and Barrow, C. J. (1999) Familial prion disease mutation alters the secondary structure of recombinant mouse prion protein: implications for the mechanism of prion formation. *Biochemistry* **38,** 3280–3284
11. Abalos, G. C., Cruite, J. T., Bellon, A., Hemmers, S., Akagi, J., Mastrianni, J. A., Williamson, R. A., and Solforosi, L. (2008) Identifying key components of the PrPC-PrPSc replicative interface. *J. Biol. Chem.* **283,** 34021–34028
12. Groveman, B. R., Kraus, A., Raymond, L. D., Dolan, M. A., Anson, K. J., Dorward, D. W., and Caughey, B. (2015) Charge neutralization of the central lysine cluster in prion protein (PrP) promotes PrP(Sc)-like folding of recombinant PrP amyloids. *J. Biol. Chem.* **290,** 1119–1128
13. Adzhubei, A. A., Sternberg, M. J., and Makarov, A. A. (2013) Polyproline-II helix in proteins: structure and function. *J. Mol. Biol.* **425,** 2100–2132
14. Eichner, T., and Radford, S. E. (2009) A generic mechanism of β2-microglobulin amyloid assembly at neutral pH involving a specific proline switch. *J. Mol. Biol.* **386,** 1312–1326
15. Eichner, T., Kalverda, A. P., Thompson, G. S., Homans, S. W., and Radford, S. E. (2011) Conformational conversion during amyloid formation at atomic resolution. *Mol. Cell* **41,** 161–172
16. Nakamura, K., Greenwood, A., Binder, L., Bigio, E. H., Denial, S., Nicholson, L., Zhou, X. Z., and Lu, K. P. (2012) Proline isomer-specific antibodies reveal the early pathogenic tau conformation in Alzheimer's disease. *Cell* **149,** 232–244
17. Rauscher, S., Baud, S., Miao, M., Keeley, F. W., and Pomès, R. (2006) Proline and glycine control protein self-organization into elastomeric or amyloid fibrils. *Structure* **14,** 1667–1676
18. Pastorino, L., Sun, A., Lu, P. J., Zhou, X. Z., Balastik, M., Finn, G., Wulf, G., Lim, J., Li, S. H., Li, X., Xia, W., Nicholson, L. K., and Lu, K. P. (2006) The prolyl isomerase Pin1 regulates amyloid precursor protein processing and amyloid-β production. *Nature* **440,** 528–534
19. Lu, P. J., Wulf, G., Zhou, X. Z., Davies, P., and Lu, K. P. (1999) The prolyl isomerase Pin1 restores the function of Alzheimer-associated phosphorylated tau protein. *Nature* **399,** 784–788
20. Smirnovas, V., Kim, J. I., Lu, X., Atarashi, R., Caughey, B., and Surewicz, W. K. (2009) Distinct structures of scrapie prion protein (PrPSc)-seeded *versus* spontaneous recombinant prion protein fibrils revealed by hydrogen/deuterium exchange. *J. Biol. Chem.* **284,** 24233–24241
21. Smirnovas, V., Baron, G. S., Offerdahl, D. K., Raymond, G. J., Caughey, B., and Surewicz, W. K. (2011) Structural organization of brain-derived mammalian prions examined by hydrogen-deuterium exchange. *Nat. Struct. Mol. Biol.* **18,** 504–506
22. Prusiner, S. B., Groth, D. F., Bolton, D. C., Kent, S. B., and Hood, L. E. (1984) Purification and structural studies of a major scrapie prion protein. *Cell* **38,** 127–134
23. Hope, J., Multhaup, G., Reekie, L. J., Kimberlin, R. H., and Beyreuther, K. (1988) Molecular pathology of scrapie-associated fibril protein (PrP) in mouse brain affected by the ME7 strain of scrapie. *Eur. J. Biochem.* **172,** 271–277
24. Lu, X., Wintrode, P. L., and Surewicz, W. K. (2007) β-Sheet core of human prion protein amyloid fibrils as determined by hydrogen/deuterium exchange. *Proc. Natl. Acad. Sci. U.S.A.* **104,** 1510–1515
25. Cobb, N. J., Sönnichsen, F. D., McHaourab, H., and Surewicz, W. K. (2007) Molecular architecture of human prion protein amyloid: a parallel, in-register β-structure. *Proc. Natl. Acad. Sci. U.S.A.* **104,** 18946–18951
26. Groveman, B. R., Dolan, M. A., Taubner, L. M., Kraus, A., Wickner, R. B., and Caughey, B. (2014) Parallel in-register intermolecular β-sheet architectures for prion-seeded prion protein (PrP) amyloids. *J. Biol. Chem.* **289,** 24129–24142
27. Wang, F., Wang, X., Yuan, C. G., and Ma, J. (2010) Generating a prion with bacterially expressed recombinant prion protein. *Science* **327,** 1132–1135

[3] B. D. Sykes, personal communication.

28. Deleault, N. R., Piro, J. R., Walsh, D. J., Wang, F., Ma, J., Geoghegan, J. C., and Supattapone, S. (2012) Isolation of phosphatidylethanolamine as a solitary cofactor for prion formation in the absence of nucleic acids. *Proc. Natl. Acad. Sci. U.S.A.* **109,** 8546–8551
29. Deleault, N. R., Harris, B. T., Rees, J. R., and Supattapone, S. (2007) Formation of native prions from minimal components *in vitro*. *Proc. Natl. Acad. Sci. U.S.A.* **104,** 9741–9746
30. Miller, M. B., Wang, D. W., Wang, F., Noble, G. P., Ma, J., Woods, V. L., Jr., Li, S., and Supattapone, S. (2013) Cofactor molecules induce structural transformation during infectious prion formation. *Structure* **21,** 2061–2068
31. Wilham, J. M., Orrú, C. D., Bessen, R. A., Atarashi, R., Sano, K., Race, B., Meade-White, K. D., Taubner, L. M., Timmes, A., and Caughey, B. (2010) Rapid end-point quantitation of prion seeding activity with sensitivity comparable to bioassays. *PLoS Pathog.* **6,** e1001217
32. Fox, B. G., and Blommel, P. G. (2009) Autoinduction of protein expression. *Curr. Protoc. Protein Sci.* Chapter 5, Unit 5.23
33. Studier, F. W. (2005) Protein production by auto-induction in high density shaking cultures. *Protein Expr. Purif.* **41,** 207–234
34. Caughey, B., Raymond, G. J., Ernst, D., and Race, R. E. (1991) N-terminal truncation of the scrapie-associated form of PrP by lysosomal protease(s): implications regarding the site of conversion of PrP to the protease-resistant state. *J. Virol.* **65,** 6597–6603
35. Caughey, B., Race, R. E., Vogel, M., Buchmeier, M. J., and Chesebro, B. (1988) *In vitro* expression in eukaryotic cells of the prion protein gene cloned from scrapie-infected mouse brain. *Proc. Natl. Acad. Sci. U.S.A.* **85,** 4657–4661
36. Edgar, R. C. (2004) MUSCLE: multiple sequence alignment with high accuracy and high throughput. *Nucleic Acids Res.* **32,** 1792–1797
37. Guindon, S., and Gascuel, O. (2003) A simple, fast, and accurate algorithm to estimate large phylogenies by maximum likelihood. *Syst. Biol.* **52,** 696–704
38. Tunnell, E., Wollman, R., Mallik, S., Cortes, C. J., Dearmond, S. J., and Mastrianni, J. A. (2008) A novel PRNP-P105S mutation associated with atypical prion disease and a rare PrPSc conformation. *Neurology* **71,** 1431–1438
39. Rogaeva, E., Zadikoff, C., Ponesse, J., Schmitt-Ulms, G., Kawarai, T., Sato, C., Salehi-Rad, S., St George-Hyslop, P., and Lang, A. E. (2006) Childhood onset in familial prion disease with a novel mutation in the PRNP gene. *Arch. Neurol.* **63,** 1016–1021
40. Jones, E. M., Surewicz, K., and Surewicz, W. K. (2006) Role of N-terminal familial mutations in prion protein fibrillization and prion amyloid propagation *in vitro*. *J. Biol. Chem.* **281,** 8190–8196
41. Jarrett, J. T., and Lansbury, P. T., Jr. (1993) Seeding "one-dimensional crystallization" of amyloid: a pathogenic mechanism in Alzheimer's disease and scrapie? *Cell* **73,** 1055–1058
42. Chou, P. Y., and Fasman, G. D. (1978) Empirical predictions of protein conformation. *Annu. Rev. Biochem.* **47,** 251–276
43. Noble, G. P., Walsh, D. J., Miller, M. B., Jackson, W. S., and Supattapone, S. (2015) Requirements for mutant and wild-type prion protein misfolding *in vitro*. *Biochemistry* **54,** 1180–1187
44. Biljan, I., Ilc, G., Giachin, G., Raspadori, A., Zhukov, I., Plavec, J., and Legname, G. (2011) Toward the molecular basis of inherited prion diseases: NMR structure of the human prion protein with V210I mutation. *J. Mol. Biol.* **412,** 660–673
45. Zahn, R., Liu, A., Lührs, T., Riek, R., von Schroetter, C., López García, F., Billeter, M., Calzolai, L., Wider, G., and Wüthrich, K. (2000) NMR solution structure of human prion protein. *Proc. Natl. Acad. Sci. U.S.A.* **97,** 145–150
46. Ilc, G., Giachin, G., Jaremko, M., Jaremko, Ł., Benetti, F., Plavec, J., Zhukov, I., and Legname, G. (2010) NMR structure of the human prion protein with the pathological Q212P mutation reveals unique structural features. *PLoS ONE* **5,** e11715
47. Shen, Y., and Bax, A. (2010) Prediction of Xaa-Pro peptide bond conformation from sequence and chemical shifts. *J. Biomol. NMR* **46,** 199–204